JOURNAL OF THERMOPHYSICS AND HEAT TRANSFER
Vol. 10, No. 4, October–December 1996

Thin-Film Thermocouples for Localized Heat Transfer Measurements

J. Lepicovsky*
NYMA, Inc., Brook Park, Ohio 44142
and
R. J. Bruckner† and F. A. Smith‡
NASA Lewis Research Center, Cleveland, Ohio 44135

This paper describes a proof-of-concept experiment on thin-film thermocouples used for localized heat transfer measurements applicable to experiments in warm turbine testing. Using thin-film thermocouples to measure turbine blade temperatures and heat transfer will noticeably improve the accuracy of the acquired data because the current method of embedded conventional thermocouples introduces large experimental uncertainty. First, we introduce the thin-film sensors and manufacturing procedures. Attention is paid to connections between thin-film thermocouples and lead wires, which have been a source of problems in the past. Then, we discuss the test arrangement and facility used for the heat transfer measurements. Finally, we present the results of bulk and local heat flux measurements, as well as overall heat transfer coefficients obtained from measurements in a narrow passage with an AR of 11.8. Experimental data acquired from thin-film thermocouples and their trends agree very well with data acquired using conventional thermocouples. The results we obtained establish confidence about using thin-film thermocouples for heat transfer measurements in warm turbine testing.

Nomenclature

Q_T = total heat transfer, W
q_B = bulk heat flow rate, kW m^{-2}
q_L = local heat flow rate, kW m^{-2}
Re_{C0} = Reynolds number, coolant side, at the entrance to the cooling passage
Re_{H3} = Reynolds number, hot-gas side, at the centerline of the test module
U_T = overall heat transfer coefficient, W K^{-1} m^{-2}
$\Delta T_{S,HC}$ = difference of hot-gas and coolant static temperatures, K

Introduction

EFFICIENT turbine blade cooling in high-performance jet engines, coupled with minimum requirements on the amount of cooling air, has recently become a critical issue in engine development. Local hot spots on turbine blades that occur because of a lack of detailed knowledge of local heat transfer coefficients on the internal walls of cooling passages can impose severe limitations on an engine's performance and structural integrity. Advances in analytical and computational techniques used to determine heat transfer and surface temperature distributions on turbine blades have led to the need to verify analytical predictions experimentally. However, the existing conventional experimental techniques are not sufficient for that purpose.

Turbine blade temperature and heat transfer measurements are presently accomplished by embedding conventional thermocouples in the blade walls. The uncertainty in this method of measurement can be as high as 50 K because of heat path distortion, uncertainty about the exact location of thermocouple junctions, and perturbation in the coolant flow pattern caused by bulky thermocouple wires very often routed through narrow cooling passages.[1] On the other hand, the recent and current development of thin-film thermocouples appears to be an ideal solution for blade and vane surface temperature measurements.[2] Very fine thin-film sensors (the overall thickness is less than 15 μm) guarantee virtually no perturbation of the heat flow path and wall thickness or of the coolant flow pattern. Thin-film sensors technology is rapidly maturing into a reliable experimental technique. Even though some recent attempts to measure the blade surface temperatures using thin-film sensors were not fully successful,[1] the failure was not caused by thin-film sensors on the blades, but by problems with the thin-film-to-lead-wire connections.

To verify and master the experimental methodology of thin-film thermocouples, we decided to first carry out experiments in a controlled test environment before applying these sensors to a warm turbine. This article reports our effort in three parts. The first part describes the thin-film sensors and manufacturing procedures. The second part addresses the test arrangement and facility used for the heat transfer measurements modeling the conditions for warm turbine tests. Finally, the results of bulk and local heat flow rate measurements are presented, as well as overall heat transfer coefficients obtained from measurements in a narrow passage with an AR of 11.8.

Thin-Film Thermocouples

Thin-film thermocouples are very fine temperature sensors (less than 15 μm thick) that are manufactured on a particular surface by a sputtering process. The technology of thin-film thermocouples was improved under several NASA Lewis Research Center (NASA LeRC) contracts.[3–5] Recently that technology was advanced even more significantly at NASA LeRC and at present is ready for applications in warm turbine testing.

Currently, the sputtering at NASA LeRC is performed in rf sputtering chambers. The sputtering material forms a part of a cathode connected to a high-voltage (up to 2400-V), high-fre-

Presented as Paper 95-2834 at the AIAA/ASME/SAE/ASEE 31st Joint Propulsion Conference and Exhibit, San Diego, CA, July 10–12, 1995; received Nov. 17, 1995; revision received March 28, 1996; accepted for publication March 28, 1996.

*Senior Supervisor, Experimental Fluid Dynamics Section. Associate Fellow AIAA.
†Operation Engineer, M/S 6-9. Member AIAA.
‡Mechanical Engineering Technician, M/S 14-3.

quency (13.56-MHz) source. During the process, molecules of the target material are knocked out of the cathode, and on their way to an anode they are deposited on a desired surface placed in their path. The sputtering is done in an argon environment at an absolute pressure level of 0.13 Pa.

Figure 1 shows a test article instrumented with four thin-film thermocouples on its external surface. The thermocouple junctions, as well as four pairs of thermocouple legs, seen in Fig. 1, are made by sputtering. A magnified view showing a typical thin-film thermocouple is shown in Fig. 2. As seen here, the sensor consists of several layers deposited on the test article surface. The manufacturing process starts with sputtering a bond coat of nickel ($\approx$2.5 μm) onto the surface.[6] The nickel significantly reduces the possibility of a sensor failure because of adherence loss. Then the process involves depositing approximately a 5-μm layer of aluminum oxide to isolate the thermocouples electrically from the substrate. However, the aluminum oxide layer must be deposited on top of the nickel immediately to prevent the nickel from oxidizing. This is accomplished using two cathodes in the sputtering chamber, one with nickel and one with aluminum oxide. After that the article is removed from the chamber, and the electrical resistance of the aluminum oxide layer must be checked; the minimum resistance to ground is 30 MΩ, if it is less than this, the process must be repeated from the beginning.

The next phase is construction of the actual thermocouple, type E (constantan–chromel) in this case. At first, a 3-μm layer of constantan is sputtered on top of the aluminum oxide layer. Then, the would-be junction and the constantan leg path are masked with a dry transparency, and the remainder of the constantan layer is chemically etched away. In the next step, half of the would-be junction is unmasked, but the constantan leg path remains covered. Now, a 1.5-μm-thick layer of chromel is deposited on the surface. This is followed by suitable masking of the chromel leg path, and then the rest of the chromel layer is etched away. After that, the masking is washed off using acetone. To protect the sensor from erosion, we can deposit a thin layer of aluminum oxide over the entire instrumented surface. This operation was not performed for the current testing, but will be for future turbine tests.

Finally, the thin-film thermocouple legs must be spliced to lead wires to connect the sensors with data acquisition equipment, which is a difficult task. An attempt to use thin-film thermocouples in an engine environment failed solely because of problems with the thin-film-to-lead-wire connections.[1] The sputtered thermocouple legs were first connected to bare 25-μm thermocouple alloy wires, which were in turn connected to 0.25-mm-insulated thermocouple lead wires. Figure 3 shows the first connection for the thermocouples on the inner wall of the test article. The bare wires were gap-welded to the thin-film legs using two parallel electrodes. To get the wires through the wall on the external surface, we inserted four aluminum oxide double-hole plugs in the wall (white circles in Fig. 3). The second connection to the insulated lead wires was made in one of the test piece flanges. Lead wires were cemented in the flange and then ground flush with the surface. After that, the bare wires were spot-welded to the lead wires (Fig. 4). To backup the electric connection, we covered the welds with electrically conductive epoxy, which proved very reliable. We did not lose any thin-film thermocouple sensors during testing.

All thin-film thermocouples for this experiment were calibrated using a National Institute of Standards and Technology traceable platinum resistance temperature detector as the standard. Calibration results were compared to the IPTS-68 and ITS-90 thermocouple standards. A review of the calibration data indicated that the thin-film thermocouples required no special treatment with respect to signal conversion and data acquisition to achieve a measurement uncertainty equivalent to standard thermocouples.

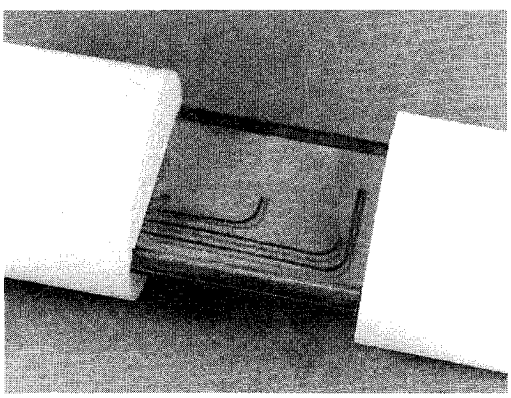

Fig. 1 Test article with four thin-film thermocouples.

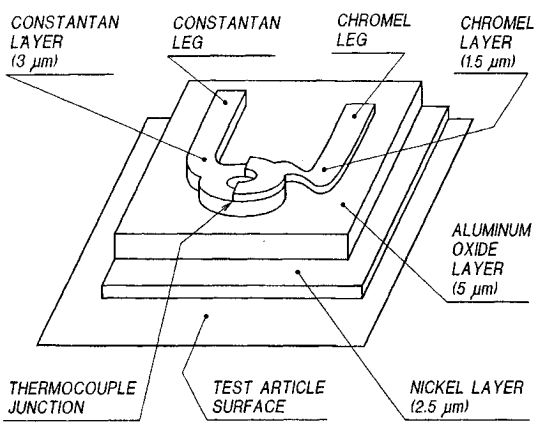

Fig. 2 Thin-film thermocouple (type E).

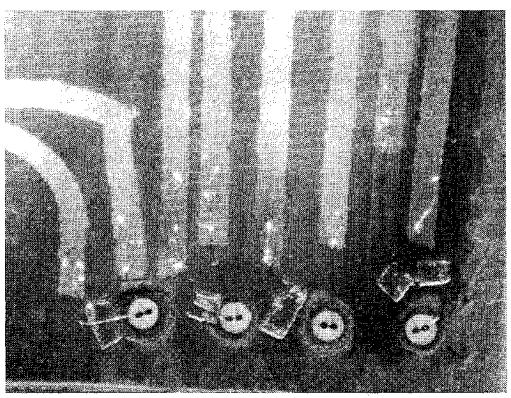

Fig. 3 Thin-film/bare lead wire connections on the inner wall of the test module.

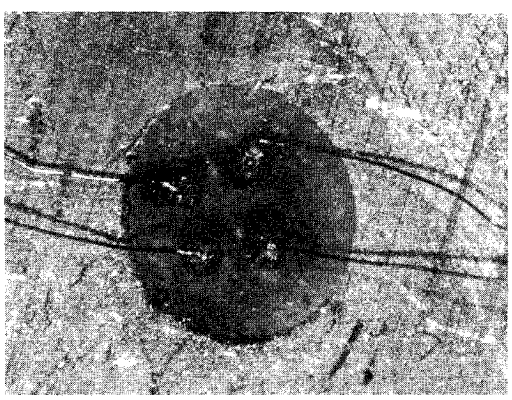

Fig. 4 Spot welds of bare and insulated thermocouple lead wires of the connection on the test module flange.

Heat Transfer Test Arrangement

The test arrangement was designed to model flow and heat transfer conditions, in terms of Reynolds and Mach numbers, typical for cooled turbine components using a simple geometry. In essence, the test article consisted of an internally cooled flat plate submerged into a stream of heated air. The principle is shown in Fig. 5. A simplified section of the test rig is depicted in Fig. 6. The photograph of Fig. 7 shows the test section with a removed sidewall to expose the cooled flat plate in the middle of the channel.

In the test rig, the heated air flows from a plenum, on the left, through the test section with a vertically located flat plate, and exits on the right into an exhaust system. The flat plate in the test section consists of a leading plate on the left, a cooled segment in the middle (the test module), and a trailing plate on the right. The leading plate is replaceable; thus, the Reynolds number of the external flow in the test module region, which is based on the distance from the leading edge, can be set to various levels at identical heated airflow conditions. Of course, the external flow Reynolds number also can be controlled by varying flow conditions and retaining the same leading plate section.

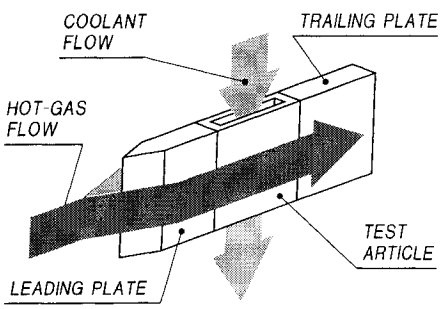

Fig. 5 Concept of heat transfer test rig.

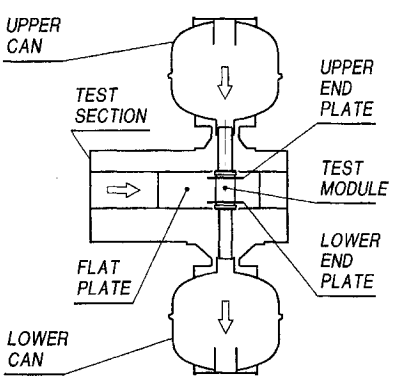

Fig. 6 Simplified section of the heat transfer test rig.

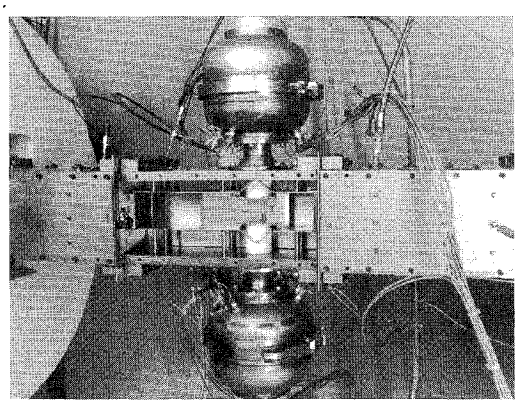

Fig. 7 Overall view of the heat transfer test rig.

Cooling air flows vertically through the inlet plenum (upper can), the test module, and the exit plenum (lower can). The coolant flow total parameters were measured in both inlet and exit plenums. Mass flow of the coolant stream was measured upstream of the inlet plenum. Both plenums were carefully insulated using Macor® lining. As we demonstrate in Fig. 8, the test module can easily be removed from the test section, allowing one to inspect and calibrate the thin-film thermocouples on the test module without major disruption of the test facility. Finally, the photograph in Fig. 9 reveals additional details of the test section, including the upper and lower end plates that determine the extent of the heat transfer area. The cross-sectional dimensions of the coolant passage are 21.0 × 1.8 mm. The size of the heat transfer area is 21.0 × 51.1 mm (heat is transferred through both walls of the test module). The

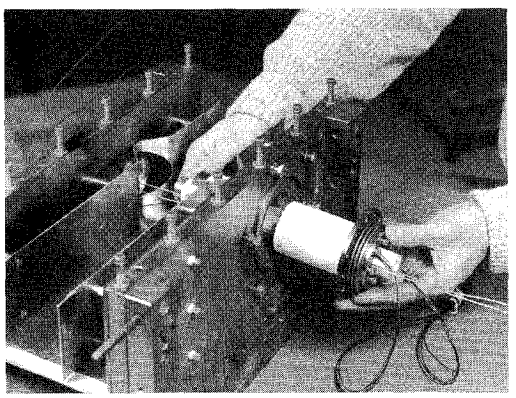

Fig. 8 Insertion of the test module into the test section.

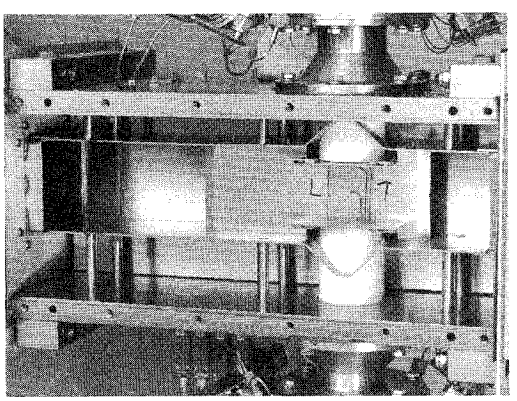

Fig. 9 Assembled test section.

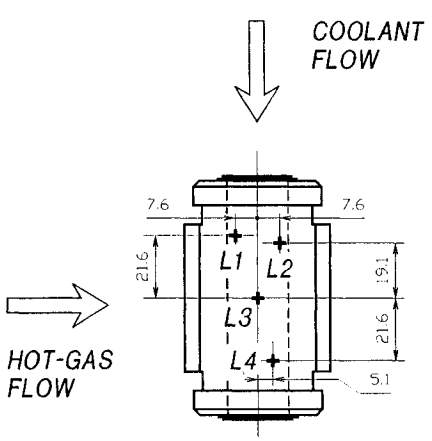

Fig. 10 Location of heat transfer sensors on the test module; the thin-film sensors are located on both external and internal surfaces (dimensions in millimeters).

Table 1 Test conditions, hot-gas side

Parameter	Test conditions I	II	III
Flow velocity, m s^{-1}	113.0 ± 2.9	162.3 ± 1.8	135.3 ± 1.2
Absolute static pressure, kPa	92.61 ± 1.11	88.64 ± 0.73	163.78 ± 1.16
Static temperature, K	379.7 ± 0.6	417.3 ± 0.5	422.5 ± 4.4
Mach number	0.29 ± 0.01	0.40 ± 0.01	0.33 ± 0.01
Reynolds number	553,600 ± 13,300	647,000 ± 8,200	976,200 ± 18,200

Table 2 Test conditions, coolant side

Mass flow rate, g s^{-1}	7.79	9.40	13.38	16.94	20.22
Flow velocity, m s^{-1}	136.1	154.5	168.4	173.6	177.6
Absolute static pressure, kPa	127.41	134.64	174.10	212.60	246.92
Static temperature, K	289.4	287.5	284.7	283.1	281.8
Mach number	0.40	0.46	0.50	0.52	0.53
Reynolds number	38,120	46,260	66,310	84,320	101,070

material of the test module is Inconel 718. The wall thickness is 1.4 mm.

The heat transfer test rig is one element of the Engine Component Instrumentation Development Facility at NASA LeRC.[7] The facility mass flow rate can range up to 1.13 kg s^{-1}, at an absolute total inlet pressure of 380 kPa and a total inlet temperature of 533 K. The facility uses electric air heaters to control the flow temperatures. The exhaust system can maintain a vacuum at 10-kPa absolute pressure level.

The test module was instrumented with four thin-film thermocouples on the external surface and four sensors on the internal surface of the same wall. Figure 10 depicts the location of the sensors on the external wall (labels L1–L4). At each location, the pair of thermocouples, known wall thickness, and known material properties constitute a well-defined local heat transfer sensor for the assumption of one-dimensional heat conduction.

Heat Transfer Measurements

The tests reported here were performed at three distinct operating conditions on the hot-gas side. The conditions are summarized in Table 1. The characteristic length in Re_{H_3} is the distance from the leading edge of the flat plate to the centerline of the test module. Only one leading-edge plate was used; the characteristic length was 126.9 mm. The hot-gas flow parameters were determined by measuring the total pressure and total temperature in the hot stream 10 mm above the surface of the test module, and the static wall pressure. Probe locations faced the test module centerline.

On the coolant side, the mass flow rate was varied in a stepwise fashion from 5 to 25 g s^{-1} by increasing the coolant inlet total pressure, which resulted in the Reynolds number range from 2.5×10^4 to 1.1×10^5. Test conditions for several Reynolds numbers Re_{C_0} are provided in Table 2. The characteristic length in the coolant Reynolds number is the hydraulic diameter of the cooling passage (3.28 mm). Total pressure and total temperature levels of the coolant flow were measured in the upper can. The measured values were used to calculate isentropic static parameters at the entrance section of the coolant passage. These parameters were used to calculate Re_{C_0}.

Two kinds of measurements were performed: 1) bulk and 2) local heat flow rates. The total heat transfer and bulk heat flow rate were determined by the difference between the total exit and inlet coolant temperatures and the coolant mass flow rate. The inlet and exit coolant total temperatures were measured by conventional thermocouples in the upper and lower coolant plenums, respectively. We assumed a one-dimensional heat conduction to determine the local heat flow rates from the wall surface temperatures (measured by the thin-film thermocouples), local wall thicknesses, and known metal heat conductivity. The wall temperatures for locations L2 and L3 indicated

Table 3 Test conditions, assignment of symbols (Figs. 11–15)

Symbol	Test condition	Parameter
□	I	$Re_{H\_3} = 976 \times 10^3$ $\Delta T_{S\_HC} = 131$ K
◇	II	$Re_{H\_3} = 647 \times 10^3$ $\Delta T_{S\_HC} = 128$ K
△	III	$Re_{H\_3} = 554 \times 10^3$ $\Delta T_{S\_HC} = 94$ K

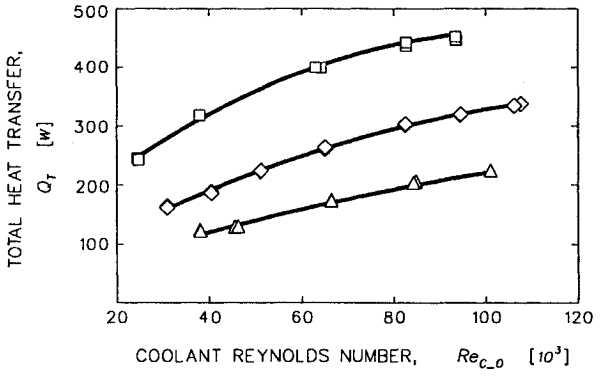

Fig. 11 Total heat transfer for the cooling passage (for symbols see Table 3).

that temperature gradients across the wall were 20–40 times larger than temperature gradients along the wall. The assumption of one-dimensional heat conduction for these locations is therefore valid.

The total heat transfer as a function of Re_{C_0}, recorded for three hot-gas-side flow conditions, is shown in Fig. 11 (Table 3). The total heat transfer increases with increasing coolant Reynolds number, hot-gas Reynolds number, and the increasing temperature difference between hot and coolant sides. The U_T for the test module is plotted in Fig. 12. The overall heat transfer coefficient was calculated from the bulk temperature rise of the cooling air, the total heat transfer area (two walls), and the difference between static temperatures for the hot-gas and coolant sides. The static temperature for the hot-gas side was calculated from measured hot-gas parameters at the test module location. The coolant static temperature was calculated for the conditions at the entrance into the cooling passage.

Our interest focused on comparison of bulk and local heat flow rate results. Figure 13 shows the average heat flow rate determined from the total heat transfer, measured on the coolant side, and the heat transfer area. Figures 14 and 15 show local heat flow rates for locations L2 and L3, respectively.

Local heat flow rates were determined from thin-film thermocouple readings across the test module wall. A rigorous comparison would require determining the distribution of local heat flow rates over the heat transfer area, averaging it, and then comparing it with the measured bulk heat flow rate. However, this could not be done because data exist for only two points (L2 and L3) over an area where the distribution of the local heat flow rates is not uniform. Nevertheless, useful conclusions can still be drawn.

Local heat flow rates in location L2 should be noticeably higher than the bulk rate for the following two reasons. The temperature difference (hot-gas vs coolant) will be larger here, and the entrance effects will be quite pronounced. On the other hand, it is reasonable to expect that the local heat flow rate at location L3 will be less than the bulk heat flow rate because the local heat flow rate distribution in the coolant flow direction is not linear. Data in Figs. 13–15 fully confirm that expectation for the two lower hot-gas side Reynolds numbers ($Re_{H\_3} = 554 \times 10^3$ and $Re_{H\_3} = 647 \times 10^3$). A summary plot

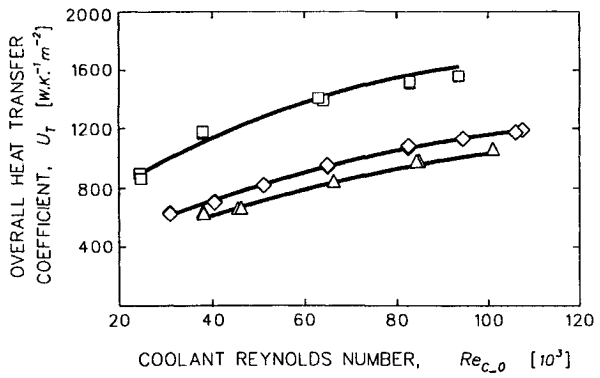

Fig. 12 Overall heat transfer coefficient for the cooling passage (for symbols see Table 3).

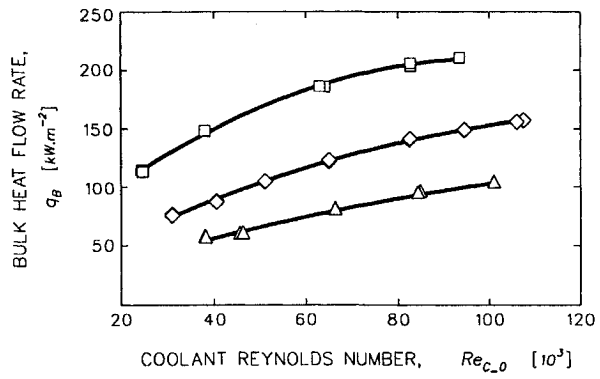

Fig. 13 Bulk heat flow rate (for symbols see Table 3).

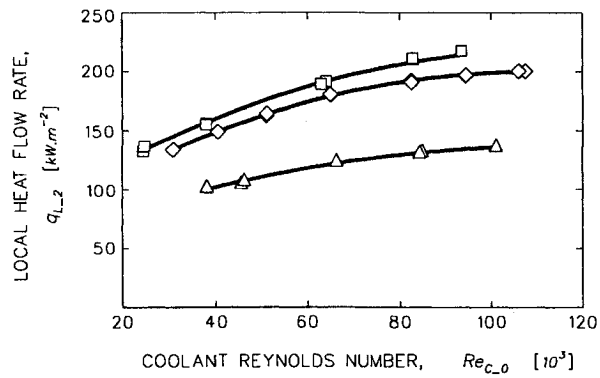

Fig. 14 Local heat flow rate at location L2, entrance to the heat transfer section (for symbols see Table 3).

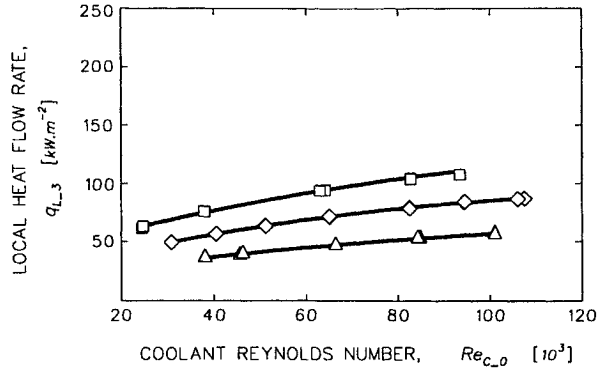

Fig. 15 Local heat flow rate at location L3, middle of the heat transfer section (for symbols see Table 3).

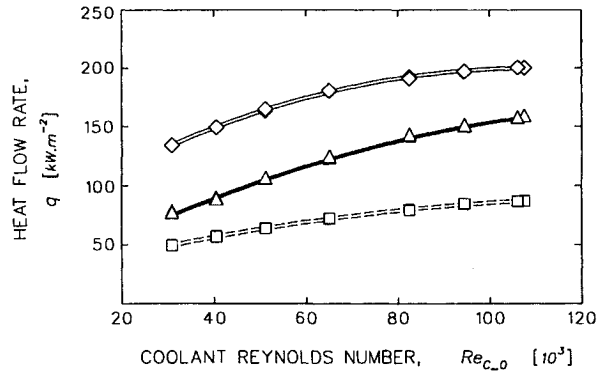

Fig. 16 Comparison of bulk and local heat flow rates at $Re_{H\_3} = 647 \times 10^3$ (solid line, bulk heat flow rate; double line, local heat flow rate at L2; broken double line, local heat flow rate at L3).

for a medium gas-side Reynolds number shown in Fig. 16 supports this discussion. For the highest gas-side Reynolds number of 976×10^3, however, the increase of the local heat flow rate at station L2 is less, relative to the bulk rate, than it was for the two lower Reynolds numbers. At present, we lack sufficient data to permit comments on this observation.

Conclusions

The following lessons and conclusions emerged during this study:

1) Most important, we developed and verified the methodology of applying thin-film thermocouples to local heat transfer measurements.

2) Advances in the thin-film technology and a novel method for splicing the thin films with thicker lead wires make it possible to apply thin-film thermocouples successfully to warm turbine testing.

3) Experimental data acquired from thin-film thermocouples (wall measurements) and their trends agree very well with data acquired on the coolant side using conventional thermocouples (bulk temperature rise).

4) Local heat transfer data obtained in the present study indicate a significant heat rate increase in the entrance region of a cooling passage.

5) Measured heat flow rates using thin-film thermocouples may serve as a database for verifying analytical predictions for heat transfer in narrow rectangular passages with a high AR.

6) The results we obtained establish confidence about using thin-film thermocouples for heat transfer measurements in warm turbine testing.

Acknowledgments

The authors are grateful to L. J. Bober of the NASA LeRC Propulsion Systems Division and K. C. Civinskas of the Turbomachinery Technology Branch for their continuing support.

References

[1]Grant, H. P., Przybyszewski, J. S., and Claing, R. G., "Turbine Blade Temperature Measurements Using Thin Film Temperature Sensors," NASA CR-165201, Jan. 1985.

[2]Englund, D. R., and Seasholtz, R. G., "Advanced High-Temperature Instrumentation for Hot Section Research Applications," *Journal of Engineering for Gas Turbines and Power*, Vol. 111, No. 1, 1989, pp. 103–113.

[3]Liebert, C. H., Mazaris, G. A., and Brandhorst, W., "Turbine Blade Metal Temperature Measurement with a Sputtered Thin Film Chromel–Alumel Thermocouple," NASA TM X-71844, Dec. 1975.

[4]Grant, H. P., and Przybyszewski, J. S., "Thin Film Temperature Sensor—Phase I," NASA CR-159782, Jan. 1985.

[5]Kim, W. S., and Barrows, R. F., "Prototype Thin-Film Thermocouple/Heat-Flux Sensor for a Ceramic-Insulated Diesel Engine," DOE/NASA/50162-1, NASA TM-100798, March 1988.

[6]Lepicovsky, J., Bruckner, R. J., and Smith, F. A., "Application of Thin-Film Thermocouples to Localized Heat Transfer Measurements," NASA TM-107045, Oct. 1995; also AIAA Paper 95-2834, July 1995.

[7]Bruckner, R. J., Buggele, A. E., and Lepicovsky, J., "Engine Component Instrumentation Development Facility at NASA Lewis Research Center," NASA TM-105644, June 1992; also AIAA Paper 92-3995, July 1992.